

Spectrally uncorrelated biphotons generated from ‘the family of BBO crystal’

Rui-Bo Jin^{1,3}, Wu-Hao Cai¹, Chunling Ding¹, Feng Mei^{3,4,*}

Guang-Wei Deng^{2,6,†}, Ryosuke Shimizu⁵, and Qiang Zhou^{2,6,‡}

¹ *Hubei Key Laboratory of Optical Information and Pattern Recognition,
Wuhan Institute of Technology, Wuhan 430205, China*

² *Institute of Fundamental and Frontier Science and School of Optoelectronic Science and Engineering,
University of Electronic Science and Technology of China, Chengdu 610054, China*

³ *State Key Laboratory of Quantum Optics and Quantum Optics Devices,
Institute of Laser Spectroscopy, Shanxi University, Taiyuan, Shanxi 030006, China*

⁴ *Collaborative Innovation Center of Extreme Optics,
Shanxi University, Taiyuan, Shanxi 030006, China*

⁵ *The University of Electro-Communications, 1-5-1 Chofugaoka, Chofu, Tokyo, Japan and*

⁶ *CAS Key Laboratory of Quantum Information, University of Science and Technology of China, Hefei 230026, China*

(Dated: December 6, 2019)

Spectrally intrinsically uncorrelated biphoton states generated from nonlinear crystals are very important but rare resources for quantum photonics and quantum information applications. Previously, such biphoton states were generated from several kinds of crystals, however, their wavelength ranges and nonlinear efficiencies were still limited for various applications. In order to explore new crystal for wider wavelength range and higher nonlinear efficiency, here we theoretically study the generation of spectrally uncorrelated biphoton states from 14 crystals in the ‘BBO family’, including BBO, CLBO, KABO, KBBF, RBBF, CBBF, BABF, BiBO, LBO, CBO, LRB4, LCB, YCOB, and GdCOB. They satisfy three kinds of group-velocity matching condition from near-infrared to telecom wavelengths. Furthermore, heralded single photons can be generated with a purity as high as 0.98, which is achieved without any narrow filtering. The indistinguishability of photons from independent sources is examined by the Hong-Ou-Mandel interference, which results in a visibility of 98% also without any further filtering, i.e., photons from different heralded single-photon sources are highly indistinguishable. Our study may provide single-photon sources with good performance for quantum information processing at near-infrared and telecom wavelengths.

PACS numbers: 42.50.Dv, 42.65.Lm, 03.65.Ud.

I. INTRODUCTION

Biphotons generated from a spontaneous parametric down-conversion (SPDC) process in a nonlinear crystal play an important role in photonic quantum information processing (QIP) [1–3]. Thanks to the energy and momentum conservation laws, the biphotons generated are generally spectrally correlated, which leads to low collection efficiency and unwanted noise photons for further application, for instance in the application of heralded single photon generation. An avenue to improve the collection efficiency and signal to noise ratio is removing the spectral correlation of generated biphoton state, i.e., spectrally uncorrelated biphotons. Recently, such biphoton states and the heralded single photons from them are on demand for many applications in QIP, for example, quantum computation [4], boson sampling [5], quantum teleportation [6] and measurement-device-independent quantum key distribution (MDIQKD) [7, 8]. Two methods have been demonstrated to remove the spectral correlations. One is spectral filtering with narrow bandpass filters, which is simple but has drawbacks

of severely decreasing the brightness and thus lowering the heralding efficiency of the heralded photon sources [9]. The second method is to design the nonlinear crystal, so as to generate spectrally uncorrelated biphotons through group-velocity-matched (GVM) conditions [10–12].

Several works have been demonstrated for spectrally uncorrelated biphotons generation using different GVM crystals at different wavelengths. For example, the KDP crystal at 830 nm has a maximal purity of 0.97 [16–18]; 11 isomorphs of KDP can also maintain high spectral purity at near-infrared and telecom wavelengths [19]; the β -barium borate (BBO) crystal at 1526 nm can achieve a maximal purity of 0.82 [10, 20–22]; the periodically poled KTP crystal (PPKTP) at 1584 nm has a maximal purity of 0.82 [23–32], and this high purity can be kept when the wavelength is tuned from 1400 nm to 1700 nm [26]; the purity for PPKTP crystals can be further improved from 0.82 to near 1 using the custom poling crystal [33–40], or even using a machine-learning framework [41]; 4 isomorphs of PPKTP can retain the properties of PPKTP, i.e., these isomorphs satisfy the GVM condition and can prepare spectrally uncorrelated biphoton state in the range of 1300 nm to 2100 nm [42–44].

Generally speaking, each nonlinear crystal has two specific GVM wavelengths to achieve high purity of around 0.97 [19], but the tunable range of those specific wavelengths is usually very narrow. In other words, these

* meifeng@sxu.edu.cn

† gwdeng@uestc.edu.cn

‡ zhouqiang@uestc.edu.cn

Name	chemical formula	axis	structure unit	point group	$\lambda_{transp.}$ (nm)	d_{max} (pm/V)
BBO	$\beta - \text{BaB}_2\text{O}_4$	uniaxial	$(\text{B}_3\text{O}_6)^{3-}$	3m	189~3500	$d_{22}=2.2$
CLBO	$\text{CsLiB}_6\text{O}_{10}$	uniaxial	$(\text{B}_3\text{O}_7)^{5-}$	42m	180~2750	$d_{36}=0.74$
KABO	$\text{K}_2\text{Al}_2\text{B}_2\text{O}_7$	uniaxial	$(\text{BO}_3)^{3-}$	32	180~3600	$d_{11}=0.45$
KBBF	$\text{KBe}_2\text{BO}_3\text{F}_2$	uniaxial	$(\text{BO}_3)^{3-}$	32	155~3700	$d_{11}=0.49$
RBBF	$\text{RbBe}_2\text{BO}_3\text{F}_2$	uniaxial	$(\text{BO}_3)^{3-}$	32	160~3550	$d_{11}=0.45$
CBBF	$\text{CsBe}_2\text{BO}_3\text{F}_2$	uniaxial	$(\text{BO}_3)^{3-}$	32	151~3700	$d_{11}=0.5$
BABF	$\text{BaAlBO}_3\text{F}_2$	uniaxial	$(\text{BO}_3)^{3-}$	$\bar{6}$	165~3000	$d_{22}=1.24$
BiBO	BiB_3O_6	biaxial	$(\text{BO}_3)^{3-}, (\text{BO}_4)^{5-}$	2	270~2730	$d_{26}=3.48$
LBO	LiB_3O_5	biaxial	$(\text{B}_3\text{O}_7)^{5-}$	mm2	155~2600	$d_{32}=0.85$
CBO	CsB_3O_5	biaxial	$(\text{B}_3\text{O}_7)^{5-}$	222	170~3000	$d_{14}=1.08$
LRB4	LiRbB_4O_7	biaxial	$(\text{B}_3\text{O}_7)^{5-}$	222	187~3468	$d_{14}=0.45$
LCB	$\text{La}_2\text{CaB}_{10}\text{O}_{19}$	biaxial	$(\text{B}_5\text{O}_{12})^{9-}$	2	185~3000	$d_{22}=1.04$
YCOB	$\text{YCa}_4\text{O}(\text{BO}_3)_3$	biaxial	$(\text{BO}_3)^{3-}$	m	202~3700	$d_{22}=2.03$
GdCOB	$\text{GdCa}_4\text{O}(\text{BO}_3)_3$	biaxial	$(\text{BO}_3)^{3-}$	m	200~3700	$d_{22}=2.23$

TABLE I. Main properties of the 14 borate crystals discussed in this work, including the chemical formula, the axis (uniaxial or biaxial), the basic structure unit, the point group, the transparency range $\lambda_{transp.}$, and the maximal nonlinear coefficient d_{max} at around 1064 nm wavelength. All the data was obtained from Refs. [13–15].

spectrally pure states can only be prepared at some wavelength points, not at the full wavelength line. The custom poling technique can maintain both high purity and wide wavelength range, but is only applied on PPKTP and limited in the telecom wavelength range, i.e., cannot cover the near-infrared or visible range [33–40]. The isomorphs of KDP increased the GVM wavelength range but with lower nonlinear efficiency [19]. Therefore, the generation of spectrally pure biphoton states from more nonlinear crystals with wider wavelength range and higher nonlinear efficiency is still a field with high demand. In this work, we investigate the possibility of generating spectrally uncorrelated biphoton state from 14 isomorphs from the ‘BBO family’, i.e., the borate crystals, which provide wider GVM wavelengths and higher nonlinear efficiency.

II. THEORY

A. Characteristics of the ‘BBO family’

The widely used borate crystals include BBO, LBO and BiBO, which were discovered in 1978, 1987, and 1995 respectively [13–15]. Besides these three crystals, there are still many other borate nonlinear optical crystals. Table I summarized 14 typical crystals from the ‘BBO family’, including 7 uniaxial and 7 biaxial crystals [13–15]. All these 7 uniaxial crystals are negative crystals with $n_e < n_o$ and the 7 biaxial crystals satisfy $n_x < n_y < n_z$. Here $n_{e(o)}$ is the refractive index for extraordinary (ordinary) ray, and $n_{x(y,z)}$ is the refractive index for X-(Y-, Z-) dielectric axis. They mainly have basic structure units of $(\text{B}_3\text{O}_6)^{3-}$, $(\text{B}_3\text{O}_7)^{5-}$, $(\text{BO}_3)^{3-}$, $(\text{BO}_4)^{5-}$ and $(\text{B}_5\text{O}_{12})^{9-}$. The point group, an important parameter determining the effective nonlinear coefficient, is including 3m, 42m, 32, and $\bar{6}$ for the uniaxial crystals,

and 2, mm2, 222, and m for the biaxial crystal. They have a wide transparent range (from UV to infrared), relative high nonlinear coefficient (up to 3.48 pm/V), high damage threshold. These crystals have important applications, particularly in the laser industry.

In the quantum information field, BBO and BiBO are well-known crystals from the ‘BBO family’. BBO crystal is widely used to generate entangled photons with high brightness [45, 46], especially in the case of beam-like configurations [47–49]. Up to now, it has been used to prepare 6, 8, 10, 12 entangled photons [50–53]. BiBO has higher nonlinear coefficients and a smaller spatial walk-off angle than the BBO crystal. BiBO has also been used in many quantum optical experiments, e.g., quantum-enhanced tomography [54], 12 photon entangled state generation [55]. In this work, we focus on the GVM conditions of these crystals, and use these crystals for spectrally uncorrelated biphoton state generation.

B. The principle of spectrally uncorrelated biphoton state generation based on GVM conditions

In the process of spontaneous parametric down-conversion (SPDC), a pump photon is probabilistically converted to a biphoton state, e.g., the signal and idler, and in this process the energy and momentum is conserved. The biphoton state $|\psi\rangle$ can be written as

$$|\psi\rangle = \int_0^\infty \int_0^\infty d\omega_s d\omega_i f(\omega_s, \omega_i) \hat{a}_s^\dagger(\omega_s) \hat{a}_i^\dagger(\omega_i) |0\rangle |0\rangle, \quad (1)$$

where ω is the angular frequency; the subscripts s and i indicate the signal and idler photon respectively; \hat{a}^\dagger is the creation operator. The joint spectral amplitude (JSA) $f(\omega_s, \omega_i)$ is the product of the pump-envelope function (PEF) $\alpha(\omega_s, \omega_i)$ and the phase-matching function (PMF)

$\phi(\omega_s, \omega_i)$, i.e.,

$$f(\omega_s, \omega_i) = \alpha(\omega_s, \omega_i) \times \phi(\omega_s, \omega_i). \quad (2)$$

The PEF is determined by the energy conservation law, and for a Gaussian-distribution, PEF can be written as [56]

$$\alpha(\omega_s, \omega_i) = \exp\left[-\frac{1}{2} \left(\frac{\omega_s + \omega_i - \omega_{p0}}{\sigma_p}\right)^2\right], \quad (3)$$

where ω_{p0} is the center wavelength of the pump; σ_p is the bandwidth of the pump, and the full-width at half-maximum (FWHM) is $\text{FWHM}_\omega = 2\sqrt{\ln(2)}\sigma_p \approx 1.67\sigma_p$.

Using wavelengths as the variables, the PEF can be rewritten as

$$\alpha(\lambda_s, \lambda_i) = \exp\left(-\frac{1}{2} \left\{ \frac{1/\lambda_s + 1/\lambda_i - 1/(\lambda_0/2)}{\Delta\lambda/[(\lambda_0/2)^2 - (\Delta\lambda/2)^2]} \right\}^2\right), \quad (4)$$

where $\lambda_0/2$ is the central wavelength of the pump; The FWHM of the pump at intensity level is $\text{FWHM}_\lambda = \frac{2\sqrt{\ln(2)}\lambda_0^2\Delta\lambda(\lambda_0^2 - \Delta\lambda^2)}{\lambda_0^4 + \Delta\lambda^4 - 2\lambda_0^2\Delta\lambda^2[1 + \ln(4)]}$. For $\Delta\lambda \ll \lambda_0$, $\text{FWHM}_\lambda \approx 2\sqrt{\ln(2)}\Delta\lambda \approx 1.67\Delta\lambda$.

The PMF function is determined by the momentum conservation law. By assuming a flat phase distribution, the PMF function can be written as [56]

$$\phi(\omega_s, \omega_i) = \text{sinc}\left(\frac{\Delta k L}{2}\right), \quad (5)$$

where L is the length of crystal; $\Delta k = k_p - k_i - k_s$ and $k = \frac{2\pi n(\lambda, \theta, \varphi)}{\lambda}$ is the wave vector; n is the refractive index; θ and φ are the phase-matching angles; θ is the polar angle and φ is the azimuth angle, as indicated in the spherical coordinate in the Appendix. According to the theoretical analysis, the shape of the PEF is determined by the GVM condition [10, 12, 26]. In this work, we study three kinds of GVM conditions as following [19],

$$\begin{aligned} \text{GVM}_1: & V_{g,p}^{-1}(\omega_p) = V_{g,s}^{-1}(\omega_s), \\ \text{GVM}_2: & V_{g,p}^{-1}(\omega_p) = V_{g,i}^{-1}(\omega_i), \\ \text{GVM}_3: & 2V_{g,p}^{-1}(\omega_p) = V_{g,i}^{-1}(\omega_i) + V_{g,s}^{-1}(\omega_s). \end{aligned} \quad (6)$$

Here $V_{g,\mu} = \frac{d\omega}{dk_\mu(\omega)} = \frac{1}{k'_\mu(\omega)}$, ($\mu = p, s, i$) is the group velocity of the pump, the signal and the idler. Under the GVM_1 , GVM_2 or GVM_3 conditions, the corresponding PMFs are distributed along the horizontal, vertical, and diagonal directions, as shown in Fig. 1(a-c). With these three kinds of GVM conditions, it is possible to prepare spectrally uncorrelated biphotons and spectrally pure heralded single photons. The JSAs with the maximal purity under these three GVM conditions are shown in Fig. 1(d-f). The corresponding maximal purity is around 0.97, 0.97, and 0.82. The purity can be calculated using Schmidt decomposition [56]. In the next section, we calculate the parameters for GVM conditions in detail [57].

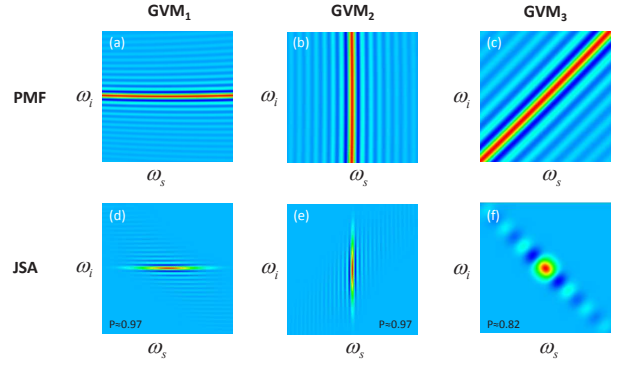


FIG. 1. The concept of three group-velocity matching (GVM) conditions. Figures in the first row show the phase-matching function (PMF) distributed along the vertical, horizontal and diagonal direction for GVM_1 , GVM_2 , and GVM_3 , respectively. The second row shows the corresponding joint spectral amplitude (JSA) with the maximal purity of around 0.97, 0.97, and 0.82 respectively.

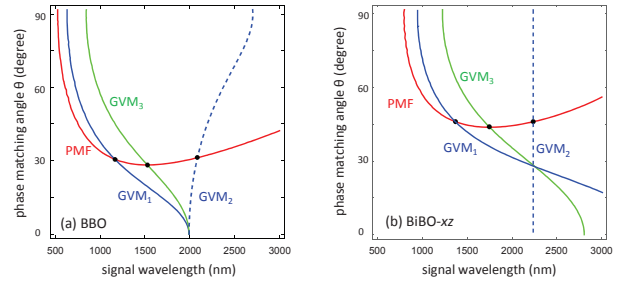


FIG. 2. The phase-matching function (PMF) and group-velocity matching functions (GVM_1 , GVM_2 , and GVM_3) for different signal wavelength λ and phase-matching angle θ for BBO crystal (a) and for BiBO crystal in the xz plane (b). In this calculation, we consider the Type-II phase-matching condition with collinear and wavelength-degenerate ($2\lambda_p = \lambda_s = \lambda_i$) configuration.

III. CALCULATION AND SIMULATION

A. Wavelength degenerate case

First, we consider the Type-II ($e \rightarrow o + e$) SPDC with collinear and wavelength-degenerate ($2\lambda_p = \lambda_s = \lambda_i$) configurations. According to the three GVM conditions, the GVM wavelength $\lambda_{p(s,i)}$ and the corresponding phase-matched angle θ can be calculated. Take BBO as an example, Fig. 2(a) shows the PMF and $\text{GVM}_{1(2,3)}$ conditions for different wavelengths and phase-matched angles. The cross points in Fig. 2 show that the PMF and GVM conditions are simultaneously satisfied at the wavelength of 1164 nm, 1526 nm, 2084 nm respectively. Following the same method, we also calculate the GVM conditions for other crystals. Table II lists the details of the three kinds of GVM conditions for 7 uniaxial crystals from the ‘BBO family’. In Tab. II, the down-converted photons have a wavelength range from 1032 to 2158 nm,

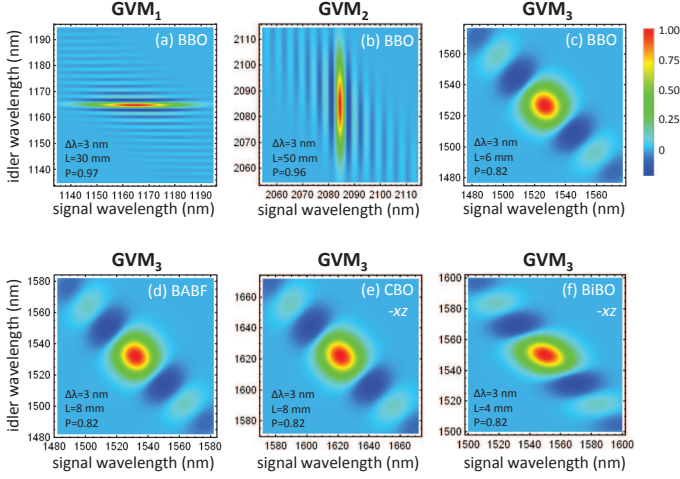


FIG. 3. The JSA of the biphotons generated from BBO, BABF, CBO, and BiBO. The bandwidth $\Delta\lambda$, the crystal length L and the purity P are listed in each figure.

and the corresponding pump wavelength range is from 516 to 1079 nm. It is noteworthy that BBO and BABF crystal can match the GVM₃ condition at 1526 nm and 1532 nm wavelength, e.g., in the C-band of telecommunication wavelength. Figure 3(a, b, c) show the JSAs of BBO crystal at its GVM_{1(2,3)} wavelengths, and the spectral purity is 0.97, 0.96, and 0.82 respectively.

For biaxial crystals, we consider the GVM conditions in different planes. Figure 2(b) shows the PMF and GVM_{1(2,3)} conditions of BiBO crystals in the xz plane for different wavelengths and phase-matched angles. The GVM_{1(2,3)} wavelengths are at 1374 nm, 2238 nm, and 1750 nm respectively. The GVM wavelengths for other crystals in different planes are listed in Tab. III. It can be found that the BiBO, LBO, and CBO crystals can satisfy the conditions in the xz plane, with $\varphi = 0^\circ$. LBO, LCB, YCOB, and GdCOB can satisfy the conditions in the yz plane, with $\varphi = 90^\circ$. CBO, LRB4, YCOB, and GdCOB can satisfy the conditions in the xy plane, with $\theta = 90^\circ$. In Tab. III, the down-converted photons have a wavelength range from 982 to 2488 nm, and the corresponding pump wavelength range is from 491 to 1244 nm. It is noteworthy that CBO in the xz plane and LRB4 in the xy plane can match the GVM₃ and GVM₂ conditions at 1622 nm and 1636 nm wavelength, i.e., in the L-band of telecommunication wavelength.

Figure 3(d) shows the JSA of BABF crystal at its GVM₃ wavelength of 1532 nm with a purity of 0.82. Figure 3(e) shows the JSA of CBO at its GVM₃ wavelength in xz plane, with the spectral purity of 0.82. Under the GVM₃ condition, the purity can be kept over 0.8 when the wavelength is tuned over 200 nm wavelength range [26]. Take BiBO crystal as an example, although the GVM₃ wavelength is 1750 nm for BiBO, the purity still can achieve 0.82 at 1550 nm, as shown in Fig 3(f). This property is very useful to increase the tunability of the pure single-photon source.

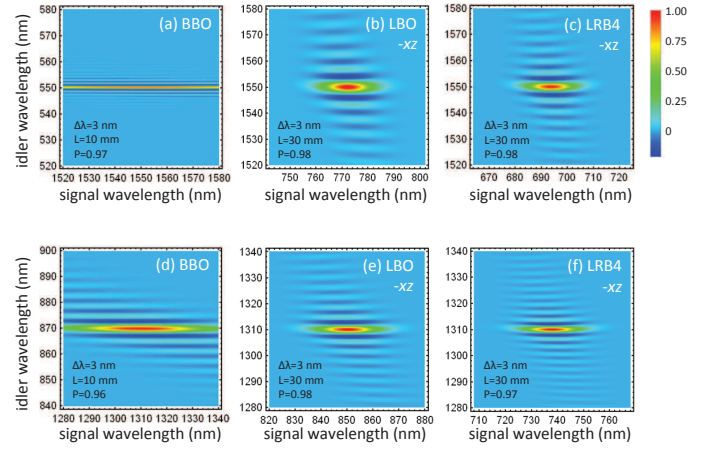


FIG. 4. The JSA of biphotons with non-degenerated wavelengths generated from BBO (a, d), LBO (b, e) and LRB4 (c, f) under the GVM₁ condition. The bandwidth $\Delta\lambda$, the crystal length L and the purity P are listed in each figure. Figures in the first (second) row are for 1550 (1310) nm wavelength.

B. Wavelength nondegenerate case

In the wavelength nondegenerate case, we consider the wavelength of the pump photons locate at 400 ~ 540 nm, which are the wavelengths for commercial-available, low-cost laser diodes. One of the down-converted photons is at 500 ~ 900 nm wavelength range, where silicon avalanche photodiode (APD) based single-photon detector has good performance. The other down-converted photon is at telecom wavelength around 1550 nm or 1310 nm, for low-loss long-distance transmission in optical fibers. The typical configurations include 405 nm \rightarrow 548 nm + 1550 nm, 520 nm \rightarrow 783 nm + 1550 nm, 405 nm \rightarrow 586 nm + 1310 nm, and 520 nm \rightarrow 862 nm + 1310 nm. These configurations are connecting the visible, near-infrared wavelength and the telecom wavelength [59–61]. In these wavelength range, our results show that 7 uniaxial and 2 biaxial crystals satisfy the GVM₁ condition in SPDC with collinear and wavelength-nondegenerated ($\lambda_s \neq \lambda_i$) configurations. Table IV lists the GVM₁ condition for BBO, CLBO, KABO, KBBF, RBBF, CBBF, BABF, LBO, and LRB4. The pump wavelength is ranging from 401 nm to 542 nm, and down-converted photons' wavelength includes the telecom wavelength of 1310 nm or 1550 nm. The JSAs under these conditions for BBO, LBO, and LRB4 are shown in Fig. 4. Each crystal can achieve the GVM₁ condition at both 1310 nm and 1550 nm. All the JSAs in Fig. 4 have a long elliptical distribution in the horizontal direction, and with high purities from 0.96 to 0.98.

C. HOM interference measurement

The quality of the spectrally uncorrelated biphoton state can be tested by Hong-Ou-Mandel (HOM) inter-

Name	GVM ₁ (purity ≈ 0.97)	GVM ₂ (purity ≈ 0.97)	GVM ₃ (purity ≈ 0.82)
BBO	$\lambda_p=582$ nm, $\lambda_{s,i}=1164$ nm $\theta=30.6^\circ$, $d_{\text{eff}}=1.46$ pm/V	$\lambda_p=1042$ nm, $\lambda_{s,i}=2084$ nm $\theta=31.2^\circ$, $d_{\text{eff}}=1.32$ pm/V	$\lambda_p=763$ nm, $\lambda_{s,i}=1526$ nm $\theta=28.3^\circ$, $d_{\text{eff}}=1.49$ pm/V
CLBO	$\lambda_p=520$ nm, $\lambda_{s,i}=1040$ nm $\theta=43.0^\circ$, $d_{\text{eff}}=0.68$ pm/V	$\lambda_p=934$ nm, $\lambda_{s,i}=1868$ nm $\theta=44.2^\circ$, $d_{\text{eff}}=0.62$ pm/V	$\lambda_p=681$ nm, $\lambda_{s,i}=1362$ nm $\theta=39.4^\circ$, $d_{\text{eff}}=0.65$ pm/V
KABO	$\lambda_p=521$ nm, $\lambda_{s,i}=1042$ nm $\theta=40.8^\circ$, $d_{\text{eff}}=0.24$ pm/V	$\lambda_p=930$ nm, $\lambda_{s,i}=1860$ nm $\theta=42.0^\circ$, $d_{\text{eff}}=0.23$ pm/V	$\lambda_p=678$ nm, $\lambda_{s,i}=1356$ nm $\theta=37.6^\circ$, $d_{\text{eff}}=0.27$ pm/V
KBBF	$\lambda_p=516$ nm, $\lambda_{s,i}=1032$ nm $\theta=28.9^\circ$, $d_{\text{eff}}=0.34$ pm/V	$\lambda_p=933$ nm, $\lambda_{s,i}=1866$ nm $\theta=29.4^\circ$, $d_{\text{eff}}=0.31$ pm/V	$\lambda_p=682$ nm, $\lambda_{s,i}=1364$ nm $\theta=26.7^\circ$, $d_{\text{eff}}=0.35$ pm/V
RBBF	$\lambda_p=533$ nm, $\lambda_{s,i}=1066$ nm $\theta=30.4^\circ$, $d_{\text{eff}}=0.32$ pm/V	$\lambda_p=974$ nm, $\lambda_{s,i}=1948$ nm $\theta=31.0^\circ$, $d_{\text{eff}}=0.29$ pm/V	$\lambda_p=708$ nm, $\lambda_{s,i}=1416$ nm $\theta=28.0^\circ$, $d_{\text{eff}}=0.32$ pm/V
CBBF	$\lambda_p=529$ nm, $\lambda_{s,i}=1058$ nm $\theta=35.6^\circ$, $d_{\text{eff}}=0.31$ pm/V	$\lambda_p=940$ nm, $\lambda_{s,i}=1880$ nm $\theta=36.2^\circ$, $d_{\text{eff}}=0.28$ pm/V	$\lambda_p=694$ nm, $\lambda_{s,i}=1388$ nm $\theta=32.8^\circ$, $d_{\text{eff}}=0.32$ pm/V
BABF*	$\lambda_p=578$ nm, $\lambda_{s,i}=1156$ nm $\theta=47.6^\circ$, $d_{\text{eff}}=0.53$ pm/V	$\lambda_p=1079$ nm, $\lambda_{s,i}=2158$ nm $\theta=49.5^\circ$, $d_{\text{eff}}=0.50$ pm/V	$\lambda_p=766$ nm, $\lambda_{s,i}=1532$ nm $\theta=43.2^\circ$, $d_{\text{eff}}=0.63$ pm/V

TABLE II. Three kinds of GVM conditions for 7 uniaxial borate crystals. $\lambda_{p(s,i)}$ is the GVM wavelength for the pump (signal, idler). θ is the phase-matching angle and d_{eff} is the effective nonlinear coefficient. Most for the d_{eff} values can be obtained from the SNLO *v70* software package, developed by AS-Photonics, LLC [58]. *The d_{eff} value for BABF is not available from SNLO, so, we calculated the d_{eff} using the method in the Appendix. The Sellmeier equations are obtained from Refs. [13–15].

Name	GVM ₁ (purity ≈ 0.97)	GVM ₂ (purity ≈ 0.97)	GVM ₃ (purity ≈ 0.82)
BiBO- xz	$\lambda_p=687$ nm, $\lambda_{s,i}=1374$ nm $\theta=46.0^\circ$, $d_{\text{eff}}=2.50$ pm/V	$\lambda_p=1119$ nm, $\lambda_{s,i}=2238$ nm $\theta=46.0^\circ$, $d_{\text{eff}}=2.30$ pm/V	$\lambda_p=875$ nm, $\lambda_{s,i}=1750$ nm $\theta=43.8^\circ$, $d_{\text{eff}}=2.48$ pm/V
LBO- xz	not satisfied	not satisfied	$\lambda_p=647$ nm, $\lambda_{s,i}=1294$ nm $\theta=4.7^\circ$, $d_{\text{eff}}=-0.64$ pm/V
CBO- xz	not satisfied	not satisfied	$\lambda_p=811$ nm, $\lambda_{s,i}=1622$ nm $\theta=6.3^\circ$, $d_{\text{eff}}=-0.21$ pm/V
LBO- yz	$\lambda_p=491$ nm, $\lambda_{s,i}=982$ nm $\theta=31.8^\circ$, $d_{\text{eff}}=-0.58$ pm/V	$\lambda_p=864$ nm, $\lambda_{s,i}=1728$ nm $\theta=33.9^\circ$, $d_{\text{eff}}=-0.52$ pm/V	not satisfied
LCB- yz	$\lambda_p=537$ nm, $\lambda_{s,i}=1074$ nm $\theta=53.3^\circ$, $d_{\text{eff}}=0.36$ pm/V	$\lambda_p=944$ nm, $\lambda_{s,i}=1888$ nm $\theta=54.4^\circ$, $d_{\text{eff}}=0.32$ pm/V	$\lambda_p=706$ nm, $\lambda_{s,i}=1412$ nm $\theta=47.9^\circ$, $d_{\text{eff}}=0.39$ pm/V
YCOB- yz	not satisfied	$\lambda_p=1244$ nm, $\lambda_{s,i}=2488$ nm $\theta=17.1^\circ$, $d_{\text{eff}}=0.14$ pm/V	not satisfied
GdCOB- yz	$\lambda_p=668$ nm, $\lambda_{s,i}=1336$ nm $\theta=48.7^\circ$, $d_{\text{eff}}=0.22$ pm/V	not satisfied	not satisfied
CBO- xy	$\lambda_p=546$ nm, $\lambda_{s,i}=1092$ nm $\varphi=5.5^\circ$, $d_{\text{eff}}=-0.23$ pm/V	$\lambda_p=1064$ nm, $\lambda_{s,i}=2128$ nm $\varphi=22.6^\circ$, $d_{\text{eff}}=-0.73$ pm/V	not satisfied
LRB4- xy *	$\lambda_p=547$ nm, $\lambda_{s,i}=1148$ nm $\varphi=62.4^\circ$, $d_{\text{eff}}=0.36$ pm/V	$\lambda_p=818$ nm, $\lambda_{s,i}=1636$ nm $\varphi=60.0^\circ$, $d_{\text{eff}}=0.39$ pm/V	$\lambda_p=705$ nm, $\lambda_{s,i}=1410$ nm $\varphi=58.2^\circ$, $d_{\text{eff}}=0.40$ pm/V
YCOB- xy	$\lambda_p=638$ nm, $\lambda_{s,i}=1276$ nm $\varphi=55.2^\circ$, $d_{\text{eff}}=0.25$ pm/V	$\lambda_p=1205$ nm, $\lambda_{s,i}=2410$ nm $\varphi=60.5^\circ$, $d_{\text{eff}}=0.06$ pm/V	$\lambda_p=842$ nm, $\lambda_{s,i}=1684$ nm $\varphi=47.1^\circ$, $d_{\text{eff}}=0.46$ pm/V
GdCOB- xy	$\lambda_p=668$ nm, $\lambda_{s,i}=1336$ nm $\varphi=68.8^\circ$, $d_{\text{eff}}=-0.01$ pm/V	not satisfied	$\lambda_p=885$ nm, $\lambda_{s,i}=1770$ nm $\varphi=56.5^\circ$, $d_{\text{eff}}=0.22$ pm/V

TABLE III. Three kinds of GVM conditions for 7 biaxial borate crystals: BiBO, LBO, and CBO with light propagating in the xz plane; LBO, LCB, YCOB, and GdCOB in the yz plane; CBO, LRB4, YCOB, and GdCOB in the xy plane. θ is the polar angle and φ is the azimuth angle. * The d_{eff} for LRB4 is calculated using the method in the Appendix, and the d_{eff} for other crystals are obtained from SNLO *v70*.

ference. There are two kinds of HOM interference, the first one is the HOM interferences using signal and idler photons from the same SPDC source, with a typical setup shown in [62]. In this case, the two-fold coincidence probability $P_2(\tau)$ as a function of the time delay τ is given by

[63–65]:

$$P_2(\tau) = \frac{1}{4} \int_0^\infty \int_0^\infty d\omega_s d\omega_i \left| [f(\omega_s, \omega_i) - f(\omega_i, \omega_s) e^{-i(\omega_s - \omega_i)\tau}] \right|^2. \quad (7)$$

The second one is the HOM interference with two independent heralded single-photon sources, with a typical

Name	GVM ₁ condition (purity ≈ 0.97)
BBO	$\lambda_p=406$ nm, $\lambda_s=1550$ nm, $\lambda_i=550$ nm, $\theta=55.2^\circ$, $d_{\text{eff}}=0.60$ pm/V
BBO	$\lambda_p=523$ nm, $\lambda_s=1310$ nm, $\lambda_i=870$ nm, $\theta=36.8^\circ$, $d_{\text{eff}}=1.24$ pm/V
CLBO	$\lambda_p=401$ nm, $\lambda_s=1310$ nm, $\lambda_i=579$ nm, $\theta=77.9^\circ$, $d_{\text{eff}}=0.27$ pm/V
KABO	$\lambda_p=403$ nm, $\lambda_s=1310$ nm, $\lambda_i=583$ nm, $\theta=68.4^\circ$, $d_{\text{eff}}=0.07$ pm/V
KBBF	$\lambda_p=542$ nm, $\lambda_s=925$ nm, $\lambda_i=1310$ nm, $\theta=25.7^\circ$, $d_{\text{eff}}=0.36$ pm/V
RBBF	$\lambda_p=417$ nm, $\lambda_s=1310$ nm, $\lambda_i=611$ nm, $\theta=45.0^\circ$, $d_{\text{eff}}=0.21$ pm/V
CBBF	$\lambda_p=414$ nm, $\lambda_s=1310$ nm, $\lambda_i=605$ nm, $\theta=54.4^\circ$, $d_{\text{eff}}=0.16$ pm/V
BABF	$\lambda_p=509$ nm, $\lambda_s=1310$ nm, $\lambda_i=833$ nm, $\theta=62.8^\circ$, $d_{\text{eff}}=0.24$ pm/V*
LBO-xz	$\lambda_p=515$ nm, $\lambda_s=772$ nm, $\lambda_i=1550$ nm, $\theta=22.0^\circ$, $d_{\text{eff}}=-0.47$ pm/V
LBO-xz	$\lambda_p=516$ nm, $\lambda_s=850$ nm, $\lambda_i=1310$ nm, $\theta=16.0^\circ$, $d_{\text{eff}}=-0.56$ pm/V
LRB4-xz	$\lambda_p=479$ nm, $\lambda_s=694$ nm, $\lambda_i=1550$ nm, $\theta=20.5^\circ$, $d_{\text{eff}}=-0.31$ pm/V*
LRB4-xz	$\lambda_p=472$ nm, $\lambda_s=738$ nm, $\lambda_i=1310$ nm, $\theta=7.1^\circ$, $d_{\text{eff}}=-0.12$ pm/V*

TABLE IV. The parameters of wavelength non-degenerated SPDC for 7 uniaxial crystals and 2 biaxial crystals. θ is the phase-matching angle and d_{eff} is the effective nonlinear coefficient. * The d_{eff} values for BABF and LRB4 are not available in SNLO *v70*, and are calculated using the method shown in the Appendix. The d_{eff} values for other crystals are taken from the SNLO *v70* software package.

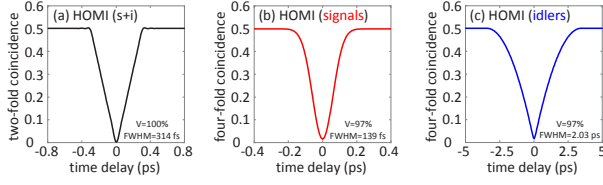


FIG. 5. (a) HOM interference curve with a signal and idler from the same BBO crystal, with the JSA shown in Fig. 3(c). (b) and (c) show the HOM interference curve with two heralded signal or idler photons from two independent BBO sources, with the JSA shown in Fig. 3(a). The visibility (V) and full-width at half-maximum (FWHM) values are labeled in each figure.

experimental setup shown in Refs. [16, 66]. In this interference, two signals s_1 and s_2 are sent to a beamsplitter for interference, and two idlers i_1 and i_2 are detected by single-photon detectors for heralding the signals. The four-fold coincidence counts P_4 as a function of τ can be described by [64, 65]

$$P_4(\tau) = \frac{1}{4} \int_0^\infty \int_0^\infty \int_0^\infty \int_0^\infty d\omega_{s_1} d\omega_{s_2} d\omega_{i_1} d\omega_{i_2} |f_1(\omega_{s_1}, \omega_{i_1}) f_2(\omega_{s_2}, \omega_{i_2}) - f_1(\omega_{s_2}, \omega_{i_1}) f_2(\omega_{s_1}, \omega_{i_2}) e^{-i(\omega_{s_2} - \omega_{s_1})\tau}|^2, \quad (8)$$

where f_1 and f_2 are the JSAs from the first and the second crystals.

Figure 5(a) is the obtained HOM interference pattern between a signal and an idler from the same BBO crystal, with the JSA shown in Fig. 3(b). Under this condition, the visibility is as high as 100%. In this case, the HOM interference visibility is determined by the exchanging symmetry of the biphotons, i.e., $f(\omega_s, \omega_i) = f(\omega_i, \omega_s)$. Figure 5(b, c) are the HOM interference curves between two heralded signals or two heralded idlers. Without using any narrow bandpass filters, visibility can achieve 98%. Please note that the visibility equals to the pu-

rity for the ideal case in the HOM interference between independent sources [16, 66, 67].

IV. DISCUSSION

In this study, we considered the GVM conditions in the main planes for biaxial crystals, i.e., in the xz , yz and xy planes, it is also possible to realize GVM conditions in an arbitrary direction. For example, previous studies have investigated phase-matching conditions and the effective nonlinear coefficient in BiBO crystal in an arbitrary direction [55, 68]. Further, we have considered the GVM condition in the collinear condition, it is also possible to realize pure-state generation in the non-collinear condition, since non-collinear configurations have been widely used in entangled photon source design [45, 46]. In addition, the ‘BBO family’ has a lot of borate crystals [13], and we only considered 14 crystals in this work, because the Sellmeier equations for many borate crystals are still not available. Therefore, to investigate the generation of spectrally uncorrelated biphotons from more borate crystals, in an arbitrary direction, in the nonlinear configuration for higher nonlinear coefficient and better wavelength range will be the future work. Especially, it is promising to study GVM conditions in BiBO crystal in the in an arbitrary direction, since this crystal has the highest nonlinear coefficient in Table I.

Designing new borate crystals with novel characteristics (e.g., higher nonlinear coefficient, smaller walk-off effect, better wavelength range) is still an active research area in the study of nonlinear optical crystals [69–71]. For example, following the anionic group theory, new nonlinear optical materials can be designed through the combination of borate and other material genomes [70, 71]. In the future, more and more borate crystals might be synthesized. Therefore, it is also possible to design and discover more borate crystals to prepare spectrally pure single-photon sources.

From the perspective of future applications, the biphotons in Fig.3(c-f) and Fig.4 can be applied for telecom wavelength; the biphotons in Fig.4 are good candidates for connecting the visible-near-infrared wavelength and telecom wavelength, which has great potential in quantum networks [72]. Crystals with GVM₁ and GVM₂ conditions can be used for interference between two signals from two independent SPDC sources. Crystals with GVM₃ condition are useful for interference between the signal and idler photons from one SPDC source. The highly pure single-photon sources at telecom wavelengths are very important for practical applications that require long-distance transmission in low-loss and low-cost optical fibers.

V. CONCLUSION

In summary, we have theoretically investigated the preparation of spectrally uncorrelated biphoton state and heralded pure single-photon state from 14 borate crystals. It was shown that these 14 crystals from the ‘BBO family’, namely BBO, CLBO, KABO, KBBF, RBBF,

CBBF, BABF, BiBO, LBO, CBO, LRB4, LCB, YCOB and GdCOB can satisfy three kinds of GVM condition from near-infrared to telecom bands. These crystals can be used to prepare spectrally uncorrelated biphoton state with purity as high as 0.98. Visibility of 100% in the HOM interference with signal and idler photons from one SPDC source, and visibility of 98% in the HOM interference between two independent SPDC sources can be achieved. This work will provide good single-photon sources for photonic quantum information from near-infrared to telecom wavelength, and will inspire people to find more crystal materials with superior properties for specific applications.

ACKNOWLEDGMENTS

This work is partially supported by the National Key R&D Program of China (Grant No. 2018YFA0307400), the National Natural Science Foundations of China (Grant Nos.91836102, 11704290, 61775025, 61704164, 61405030), and by the Program of State Key Laboratory of Quantum Optics and Quantum Optics Devices (No: KF201813).

-
- [1] S. Slussarenko and G. J. Pryde, “Photonic quantum information processing: A concise review,” *Appl. Phys. Rev.* **6**, 041303 (2019).
 - [2] F. Flamini, N. Spagnolo, and F. Sciarrino, “Photonic quantum information processing: a review,” *Rep. Prog. Phys.* **82**, 016001 (2018).
 - [3] C. Couteau, “Spontaneous parametric down-conversion,” *Contemp. Phys.* **59**, 291–304 (2018).
 - [4] I. A. Walmsley and M. G. Raymer, “Toward quantum-information processing with photons,” *Science* **307**, 1733– (2005).
 - [5] M. A. Broome, A. Fedrizzi, S. Rahimi-Keshari, J. Dove, S. Aaronson, T. C. Ralph, and A. G. White, “Photonic boson sampling in a tunable circuit,” *Science* **339**, 794 (2013).
 - [6] R. Valivarthi, M. G. Puigibert, Q. Zhou, G. H. Aguilar, V. B. Verma, F. Marsili, M. D. Shaw, S. W. Nam, D. Oblak, and W. Tittel, “Quantum teleportation across a metropolitan fibre network,” *Nature Photon.* **10**, 676 (2016).
 - [7] H.-K. Lo, M. Curty, and B. Qi, “Measurement-device-independent quantum key distribution,” *Phys. Rev. Lett.* **108**, 130503 (2012).
 - [8] R. Valivarthi, Q. Zhou, C. John, F. Marsili, V. B. Verma, M. D. Shaw, S. W. Nam, D. Oblak, and W. Tittel, “A cost-effective measurement-device-independent quantum key distribution system for quantum networks,” *Quantum Sci. Technol.* **2**, 04LT01 (2017).
 - [9] E. Meyer-Scott, N. Montaut, J. Tiedau, L. Sansoni, H. Herrmann, T. J. Bartley, and C. Silberhorn, “Limits on the heralding efficiencies and spectral purities of spectrally filtered single photons from photon-pair sources,” *Phys. Rev. A* **95**, 061803 (2017).
 - [10] W. P. Grice, A. B. U’Ren, and I. A. Walmsley, “Eliminating frequency and space-time correlations in multiphoton states,” *Phys. Rev. A* **64**, 063815 (2001).
 - [11] F. König and F. N. C. Wong, “Extended phase matching of second-harmonic generation in periodically poled KTiOPO₄ with zero group-velocity mismatch,” *Appl. Phys. Lett.* **84**, 1644 (2004).
 - [12] K. Edamatsu, R. Shimizu, W. Ueno, R.-B. Jin, F. Kaneda, M. Yabuno, H. Suzuki, S. Nagano, A. Syouji, and K. Suizu, “Photon pair sources with controlled frequency correlation,” *Prog. Inform.* **8**, 19–26 (2011).
 - [13] C. Chen, T. Sasaki, R. Li, Y. Wu, Z. Lin, Y. Mori, Z. Hu, J. Wang, G. Aka, M. Yoshimura, and Y. Kaneda, *Nonlinear Optical Borate Crystals: Principles and Applications* (Wiley-VCH Verlag GmbH & Co. KGaA, 2012).
 - [14] V. G. Dmitriev, G. G. Gurzadyan, and D. N. Nikogosyan, *Handbook of Nonlinear Optical Crystals* (Springer-Verlag Berlin Heidelberg, 1999), 3rd ed.
 - [15] D. N. Nikogosyan, *Nonlinear Optical Crystals: A Complete Survey* (Springer-Verlag, 2005).
 - [16] P. J. Mosley, J. S. Lundeen, B. J. Smith, P. Wasylczyk, A. B. U’Ren, C. Silberhorn, and I. A. Walmsley, “Heralded generation of ultrafast single photons in pure quantum states,” *Phys. Rev. Lett.* **100**, 133601 (2008).
 - [17] R.-B. Jin, J. Zhang, R. Shimizu, N. Matsuda, Y. Mitsumori, H. Kosaka, and K. Edamatsu, “High-visibility nonclassical interference between intrinsically pure heralded single photons and photons from a weak coherent field,” *Phys. Rev. A* **83**, 031805 (2011).
 - [18] R.-B. Jin, R. Shimizu, F. Kaneda, Y. Mitsumori, H. Kosaka, and K. Edamatsu, “Entangled-state generation with an intrinsically pure single-photon source and a weak coherent source,” *Phys. Rev. A* **88**, 012324 (2013).

- [19] R.-B. Jin, N. Cai, Y. Huang, X.-Y. Hao, S. Wang, F. Li, H.-Z. Song, Q. Zhou, and R. Shimizu, "Theoretical investigation of a spectrally pure-state generation from isomorphs of KDP crystal at near-infrared and telecom wavelengths," *Phys. Rev. Appl.* **11**, 034067 (2019).
- [20] T. Lutz, P. Kolenderski, and T. Jennewein, "Toward a downconversion source of positively spectrally correlated and decorrelated telecom photon pairs," *Opt. Lett.* **38**, 697–699 (2013).
- [21] T. Lutz, P. Kolenderski, and T. Jennewein, "Demonstration of spectral correlation control in a source of polarization-entangled photon pairs at telecom wavelength," *Opt. Lett.* **39**, 1481–1484 (2014).
- [22] T. Li, S. Sakurai, K. Kasai, L. Wang, M. Watanabe, and Y. Zhang, "Experimental observation of three-photon interference between a two-photon state and a weak coherent state on a beam splitter," *Opt. Express* **26**, 20442–20449 (2018).
- [23] P. G. Evans, R. S. Bennink, W. P. Grice, T. S. Humble, and J. Schaake, "Bright source of spectrally uncorrelated polarization-entangled photons with nearly single-mode emission," *Phys. Rev. Lett.* **105**, 253601 (2010).
- [24] T. Gerrits, M. J. Stevens, B. Baek, B. Calkins, A. Lita, S. Glancy, E. Knill, S. W. Nam, R. P. Mirin, R. H. Hadfield, R. S. Bennink, W. P. Grice, S. Dorenbos, T. Zijlstra, T. Klapwijk, and V. Zwiller, "Generation of degenerate, factorizable, pulsed squeezed light at telecom wavelengths," *Opt. Express* **19**, 24434–24447 (2011).
- [25] A. Eckstein, A. Christ, P. J. Mosley, and C. Silberhorn, "Highly efficient single-pass source of pulsed single-mode twin beams of light," *Phys. Rev. Lett.* **106**, 013603 (2011).
- [26] R.-B. Jin, R. Shimizu, K. Wakui, H. Benichi, and M. Sasaki, "Widely tunable single photon source with high purity at telecom wavelength," *Opt. Express* **21**, 10659–10666 (2013).
- [27] Y. Li, Z.-Y. Zhou, D.-S. Ding, and B.-S. Shi, "CW-pumped telecom band polarization entangled photon pair generation in a Sagnac interferometer," *Opt. Express* **23**, 28792–28800 (2015).
- [28] R.-B. Jin and R. Shimizu, "Extended Wiener-Khinchin theorem for quantum spectral analysis," *Optica* **5**, 93–98 (2018).
- [29] C. Greganti, P. Schiansky, I. A. Calafell, L. M. Procopio, L. A. Rozema, and P. Walther, "Tuning single-photon sources for telecom multi-photon experiments," *Opt. Express* **26**, 3286–3302 (2018).
- [30] E. Meyer-Scott, N. Prasanna, C. Eigner, V. Quiring, J. M. Donohue, S. Barkhofen, and C. Silberhorn, "High-performance source of spectrally pure, polarization entangled photon pairs based on hybrid integrated-bulk optics," *Opt. Express* **26**, 32475–32490 (2018).
- [31] H. Terashima, S. Kobayashi, T. Tsubakiyama, and K. Sanaka, "Quantum interferometric generation of polarization entangled photons," *Sci. Rep.* **8**, 15733 (2018).
- [32] Q.-Y. Zhang, G.-T. Xue, P. Xu, Y.-X. Gong, Z. Xie, and S. Zhu, "Manipulation of tripartite frequency correlation under extended phase matchings," *Phys. Rev. A* **97**, 022327 (2018).
- [33] A. M. Brańczyk, A. Fedrizzi, T. M. Stace, T. C. Ralph, and A. G. White, "Engineered optical nonlinearity for quantum light sources," *Opt. Express* **19**, 55–65 (2011).
- [34] P. B. Dixon, J. H. Shapiro, and F. N. C. Wong, "Spectral engineering by Gaussian phase-matching for quantum photonics," *Opt. Express* **21**, 5879–5890 (2013).
- [35] A. Dosseva, L. Cincio, and A. M. Brańczyk, "Shaping the joint spectrum of down-converted photons through optimized custom poling," *Phys. Rev. A* **93**, 013801 (2016).
- [36] J.-L. Tambasco, A. Boes, L. G. Helt, M. J. Steel, and A. Mitchell, "Domain engineering algorithm for practical and effective photon sources," *Opt. Express* **24**, 19616–19626 (2016).
- [37] C. Chen, C. Bo, M. Y. Niu, F. Xu, Z. Zhang, J. H. Shapiro, and F. N. C. Wong, "Efficient generation and characterization of spectrally factorable biphotons," *Opt. Express* **25**, 7300–7312 (2017).
- [38] F. Graffitti, J. Kelly-Massicotte, A. Fedrizzi, and A. M. Brańczyk, "Design considerations for high-purity heralded single-photon sources," *Phys. Rev. A* **98**, 053811 (2018).
- [39] F. Graffitti, P. Barrow, M. Proietti, D. Kundys, and A. Fedrizzi, "Independent high-purity photons created in domain-engineered crystals," *Optica* **5**, 514–517 (2018).
- [40] C. Chen, J. E. Heyes, K.-H. Hong, M. Y. Niu, A. E. Lita, T. Gerrits, S. W. Nam, J. H. Shapiro, and F. N. C. Wong, "Indistinguishable single-mode photons from spectrally engineered biphotons," *Opt. Express* **27**, 11626–11634 (2019).
- [41] C. Cui, R. Arian, S. Guha, N. Peyghambarian, Q. Zhuang, and Z. Zhang, "Wave-function engineering for spectrally uncorrelated biphotons in the telecommunication band based on a machine-learning framework," *Phys. Rev. Appl.* **12**, 034059 (2019).
- [42] R.-B. Jin, P. Zhao, P. Deng, and Q.-L. Wu, "Spectrally pure states at telecommunications wavelengths from periodically poled MTiOXO₄ (M = K, Rb, Cs; X = P, As) crystals," *Phys. Rev. Appl.* **6**, 064017 (2016).
- [43] F. Laudenbach, R.-B. Jin, C. Greganti, M. Hentschel, P. Walther, and H. Hubel, "Numerical investigation of photon-pair generation in periodically poled MTiOXO₄ (M=K, Rb, Cs; X=P, As)," *Phys. Rev. Appl.* **8**, 024035 (2017).
- [44] R.-B. Jin, G.-Q. Chen, F. Laudenbach, S. Zhao, and P.-X. Lu, "Thermal effects of the quantum states generated from the isomorphs of PPKTP crystal," *Opt. Laser Technol.* **109**, 222–226 (2019).
- [45] P. G. Kwiat, K. Mattle, H. Weinfurter, A. Zeilinger, A. V. Sergienko, and Y. Shih, "New high-intensity source of polarization-entangled photon pairs," *Phys. Rev. Lett.* **75**, 4337–4341 (1995).
- [46] P. G. Kwiat, E. Waks, A. G. White, I. Appelbaum, and P. H. Eberhard, "Ultrabright source of polarization-entangled photons," *Phys. Rev. A* **60**, R773–R776 (1999).
- [47] S. Takeuchi, "Beamlike twin-photon generation by use of type ii parametric downconversion," *Opt. Lett.* **26**, 843–845 (2001).
- [48] X.-L. Niu, Y.-F. Huang, G.-Y. Xiang, G.-C. Guo, and Z. Y. Ou, "Beamlike high-brightness source of polarization-entangled photon pairs," *Opt. Lett.* **33**, 968–970 (2008).
- [49] X.-Y. Xu, Q.-Q. Wang, W.-W. Pan, K. Sun, J.-S. Xu, G. Chen, J.-S. Tang, M. Gong, Y.-J. Han, C.-F. Li, and G.-C. Guo, "Measuring the winding number in a large-scale chiral quantum walk," *Phys. Rev. Lett.* **120**, 260501 (2018).
- [50] C.-Y. Lu, X.-Q. Zhou, O. Guhne, W.-B. Gao, J. Zhang, Z.-S. Yuan, A. Goebel, T. Yang, and J.-W. Pan, "Ex-

- perimental entanglement of six photons in graph states,” *Nat. Phys.* **3**, 91–95 (2007).
- [51] Y.-F. Huang, B.-H. Liu, L. Peng, Y.-H. Li, L. Li, C.-F. Li, and G.-C. Guo, “Experimental generation of an eight-photon greenberger-horne-zeilinger state,” *Nature Commun.* **2**, 546 (2011).
- [52] X.-C. Yao, T.-X. Wang, P. Xu, H. Lu, G.-S. Pan, X.-H. Bao, C.-Z. Peng, C.-Y. Lu, Y.-A. Chen, and J.-W. Pan, “Observation of eight-photon entanglement,” *Nat Photon* **6**, 225–228 (2012).
- [53] H.-S. Zhong, Y. Li, W. Li, L.-C. Peng, Z.-E. Su, Y. Hu, Y.-M. He, X. Ding, W. Zhang, H. Li, L. Zhang, Z. Wang, L. You, X.-L. Wang, X. Jiang, L. Li, Y.-A. Chen, N.-L. Liu, C.-Y. Lu, and J.-W. Pan, “12-photon entanglement and scalable scattershot boson sampling with optimal entangled-photon pairs from parametric down-conversion,” *Phys. Rev. Lett.* **121**, 250505 (2018).
- [54] X.-Q. Zhou, H. Cable, R. Whittaker, P. Shadbolt, J. L. O’Brien, and J. C. F. Matthews, “Quantum-enhanced tomography of unitary processes,” *Optica* **2**, 510–516 (2015).
- [55] L.-K. Chen, Z.-D. Li, X.-C. Yao, M. Huang, W. Li, H. Lu, X. Yuan, Y.-B. Zhang, X. Jiang, C.-Z. Peng, L. Li, N.-L. Liu, X. Ma, C.-Y. Lu, Y.-A. Chen, and J.-W. Pan, “Observation of ten-photon entanglement using thin BiB_3O_6 crystals,” *Optica* **4**, 77–83 (2017).
- [56] P. J. Mosley, J. S. Lundeen, B. J. Smith, and I. A. Walmsley, “Conditional preparation of single photons using parametric downconversion: a recipe for purity,” *New J. Phys.* **10**, 093011 (2008).
- [57] “See Supplemental Material at [URL will be inserted by publisher] for the original Mathematica codes which show the details of the calculation.”
- [58] A. Smith, “SNLO,” <http://www.as-photonics.com/snlo>.
- [59] F. Kaneda, K. Garay-Palmett, A. B. U’Ren, and P. G. Kwiat, “Heralded single-photon source utilizing highly nondegenerate, spectrally factorable spontaneous parametric downconversion,” *Opt. Express* **24**, 10733–10747 (2016).
- [60] E. Saglamyurek, N. Sinclair, J. Jin, J. A. Slater, D. Oblak, F. Bussières, M. George, R. Ricken, W. Sohler, and W. Tittel, “Broadband waveguide quantum memory for entangled photons,” *Nature* **469**, 512–515 (2011).
- [61] E. Saglamyurek, M. Grimaud Puigibert, Q. Zhou, L. Giner, F. Marsili, V. B. Verma, S. Woo Nam, L. Oesterling, D. Nippa, D. Oblak, and W. Tittel, “A multiplexed light-matter interface for fibre-based quantum networks,” *Nature Commun.* **7**, 11202 (2016).
- [62] C. K. Hong, Z. Y. Ou, and L. Mandel, “Measurement of subpicosecond time intervals between two photons by interference,” *Phys. Rev. Lett.* **59**, 2044–2046 (1987).
- [63] I. A. Grice, W. P. & Walmsley, “Spectral information and distinguishability in type-II down-conversion with a broadband pump,” *Phys. Rev. A* **56**, 1627–1634 (1997).
- [64] Z.-Y. J. Ou, *Multi-photon quantum interference* (Springer, 2007).
- [65] R.-B. Jin, T. Gerrits, M. Fujiwara, R. Wakabayashi, T. Yamashita, S. Miki, H. Terai, R. Shimizu, M. Takeoka, and M. Sasaki, “Spectrally resolved Hong-Ou-Mandel interference between independent photon sources,” *Opt. Express* **23**, 28836–28848 (2015).
- [66] R.-B. Jin, K. Wakui, R. Shimizu, H. Benichi, S. Miki, T. Yamashita, H. Terai, Z. Wang, M. Fujiwara, and M. Sasaki, “Nonclassical interference between independent intrinsically pure single photons at telecommunication wavelength,” *Phys. Rev. A* **87**, 063801 (2013).
- [67] H. Takesue, “Entangled photon pair generation using silicon wire waveguides,” *IEEE J. Sel. Top. Quantum Electron.* **18**, 1722–1732 (2012).
- [68] A. Halevy, E. Megidish, L. Dovrat, H. Eisenberg, P. Becker, and L. Bohaty, “The biaxial nonlinear crystal BiB_3O_6 as a polarization entangled photon source using non-collinear type-II parametric down-conversion,” *Opt. Express* **19**, 20420–20434 (2011).
- [69] Y. Yang, X. Jiang, Z. Lin, and Y. Wu, “Borate-based ultraviolet and deep-ultraviolet nonlinear optical crystals,” *Crystals* **7**, 95 (2017).
- [70] L. Kang, F. Liang, P. Gong, Z. Lin, F. Liu, and B. Huang, “Two novel deep-ultraviolet nonlinear optical crystals with shorter phase-matching second harmonic generation than $\text{KBe}_2\text{BO}_3\text{F}_2$: A first-principles prediction,” *Phys. Status Solidi RRL* **12**, 1800276 (2018).
- [71] X. Zhang, H. Wu, S. Cheng, G. Han, Z. Yang, and S. Pan, “ $\text{K}_9[\text{B}_4\text{O}_5(\text{OH})_4]_3(\text{CO}_3)\text{X}_7\text{H}_2\text{O}$ ($\text{X} = \text{Cl}, \text{Br}$): Syntheses, characterizations, and theoretical studies of noncentrosymmetric halogen borate-carbonates with short UV cutoff edges,” *Inorg. Chem.* **58**, 6974–6982 (2019).
- [72] N. Sangouard, C. Simon, H. de Riedmatten, and N. Gisin, “Quantum repeaters based on atomic ensembles and linear optics,” *Rev. Mod. Phys.* **83**, 33–80 (2011).
- [73] D. N. Nikogosyan, “Beta barium borate (BBO),” *Appl. Phys. A Solids Surf.* **52**, 359–368 (1991).
- [74] J. E. Midwinter and J. Warner, “The effects of phase matching method and of uniaxial crystal symmetry on the polar distribution of second-order non-linear optical polarization,” *Br. J. Appl. Phys.* **16**, 1135–1142 (1965).
- [75] I. Shoji, H. Nakamura, K. Ohdaira, T. Kondo, R. Ito, T. Okamoto, K. Tatsuki, and S. Kubota, “Absolute measurement of second-order nonlinear-optical coefficients of $\beta\text{-BaB}_2\text{O}_4$ for visible to ultraviolet second-harmonic wavelengths,” *J. Opt. Soc. Am. B* **16**, 620 (1999).
- [76] D. Roberts, “Simplified characterization of uniaxial and biaxial nonlinear optical crystals: a plea for standardization of nomenclature and conventions,” *IEEE J. Quantum Electron.* **28**, 2057–2074 (1992).
- [77] V. Dmitriev and D. Nikogosyan, “Effective nonlinearity coefficients for three-wave interactions in biaxial crystal of mm2 point group symmetry,” *Opt. Commun.* **95**, 173–182 (1993).

APPENDIX

A1: Coordinate for uniaxial and biaxial crystals in the calculation

Figure 6 shows the refractive index coordinate for uniaxial and biaxial crystals in the calculation. θ is the polar angle and φ is the azimuth angle.

A2: Calculation of effective nonlinear coefficient

In this section, we discuss how to calculate the effective nonlinear coefficient (d_{eff}) for uniaxial and biaxial

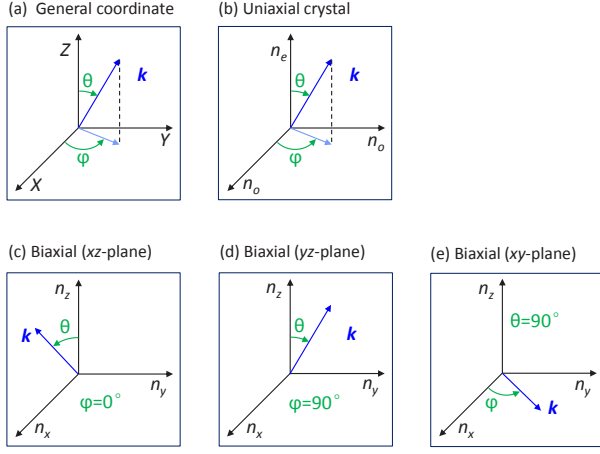


FIG. 6. The refractive index coordinate for uniaxial and biaxial crystals in the calculation. (a) is a general coordinate; (b) is the refractive index coordinate for uniaxial crystals. (c-e) are refractive index coordinate for biaxial crystals in the xz , yz and xy planes.

crystals. Firstly, we consider the uniaxial crystals and take BBO crystal as an example.

The d_{eff} value is determined by point group and phase-matching condition. For BBO crystal with a point group 3m [73], under the Type-II phase-matching condition, the d_{eff} could be calculated using the following equation [14, 74]:

$$d_{eff}(\text{BBO}) = d_{22} \cos^2(\theta + \rho) \cos(3\varphi). \quad (9)$$

In order to maximize d_{eff} , the item $\cos(3\varphi)$ should reach a maximum value, i.e, $\cos(3\varphi) = 1$ for $\varphi = 0^\circ$ or 120° . ρ

is the walk-off angle, which can be expressed as [14]:

$$\rho(\theta) = \pm \arctan\left[\frac{n_o^2(\lambda)}{n_e^2(\lambda)} \tan(\theta)\right] \mp \theta, \quad (10)$$

where the upper (lower) signs are for negative (positive) crystals. For BBO, a negative crystal, the equation is:

$$\rho(\theta)(\text{BBO}) = \arctan\left[\frac{n_o^2(\lambda)}{n_e^2(\lambda)} \tan(\theta)\right] - \theta. \quad (11)$$

Finally, we can obtain d_{eff} by substituting the value of $d_{22} = 2.2$ pm/V [75], phase-matching angle, and wavelength into the above equation.

For uniaxial crystals, we take LBO and BiBO as two examples to calculate the d_{eff} . LBO is a negative biaxial crystal with the point group of mm2, $d_{31} = -0.67$ pm/V, and $d_{32} = 0.85$ pm/V [76]. Under the type-II phase-matching condition, the expression of d_{eff} on the yz plane and xz plane can be calculated as follow [14, 77]:

xz -plane:

$$d_{eff}(\text{LBO}-xz) = d_{32} \sin^2(\theta + \rho) + d_{31} \cos^2(\theta + \rho). \quad (12)$$

yz - plane:

$$d_{eff}(\text{LBO}-yz) = d_{31} \cos(\theta + \rho). \quad (13)$$

For BiBO crystal, a negative biaxial crystal with the point group of 2 and $d_{26} = 3.48$ pm/V, the d_{eff} on the xz plane is determined by [13]:

$$d_{eff}(\text{BiBO}-xz) = d_{26} \cos(\theta + \rho). \quad (14)$$